

# Seismic response of smart nanocomposite cylindrical shell conveying fluid flow using HDQ-Newmark methods

Abbas Zamani, Reza Kolahchi\* and Mahmood Rabani Bidgoli

Department of Civil Engineering, Jasb Branch, Islamic Azad University, Jasb, Iran

(Received June 24, 2017, Revised July 28, 2017, Accepted August 1, 2017)

**Abstract.** In this research, seismic response of pipes is examined by applying nanotechnology and piezoelectric materials. For this purpose, a pipe is considered which is reinforced by carbon nanotubes (CNTs) and covered with a piezoelectric layer. The structure is subjected to the dynamic loads caused by earthquake and the governing equations of the system are derived using mathematical model via cylindrical shell element and Mindlin theory. Navier-Stokes equation is employed to calculate the force due to the fluid in the pipe. Mori-Tanaka approach is used to estimate the equivalent material properties of the nanocomposite and to consider the effect of the CNTs agglomeration on the seismic response of the structure. Moreover, the dynamic displacement of the structure is extracted using harmonic differential quadrature method (HDQM) and Newmark method. The main goal of this research is the analysis of the seismic response using piezoelectric layer and nanotechnology. The results indicate that reinforcing the pipeline by CNTs leads to a reduction in the displacement of the structure during an earthquake. Also the negative voltage applied to the piezoelectric layer reduces the dynamic displacement.

**Keywords:** dynamic analysis; nanocomposite pipes; piezoelectric layer; agglomeration; HDQM

## 1. Introduction

Cylindrical shells can be used extensively in many engineering fields such as mechanical, chemical, aerospace, civil, nuclear and so forth. For example, in automotive industry the body of the automobiles and also in oil and gas industry the pressure vessels are the obvious cases of application of cylindrical shells.

Linear and nonlinear vibrations of cylindrical shells have been investigated by many researchers. Considering the nonlinear terms in motion equations can increase the accuracy of the calculations. Most investigations on cylindrical shells conveying fluid were done by Amabili (2003). The effect of flowing fluid in cylindrical shells was studied by many researchers such as Païdoussis and Denise (1972), Weaver and Unny (1973), Païdoussis *et al.* (2003) and Amabili and Garziera (2002). The static and free vibration analysis of three-layer composite shells was performed by Maturi *et al.* (2015) using radial basis functions collocation, according to a new layerwise theory that considers independent layer rotations. The static and free vibration analysis of doubly-curved laminated shells was performed by Ferreira *et al.* (2016) using radial basis functions collocation.

In none of mentioned investigations, the structure is smart or nanocomposite. Ghorbanpour *et al.* (2011) studied the effect of material inhomogeneity on the behavior of the smart piezoelectric cylinder by applying analytical method.

Dynamic stability response of an embedded

piezoelectric nanoplate made of polyvinylidene fluoride (PVDF) was presented by Kolahchi *et al.* (2016a) based on differential cubature method (DCM) in conjunction with the Bolotin's method. Dynamic elasticity solution for a clamped, laminated cylindrical shell with two orthotropic layers bounded with a piezoelectric layer and subjected to exponential dynamic load distributed on inner surface was presented by Saviz (2015). The active vibration control of carbon nanotube (CNT) reinforced functionally graded composite cylindrical shell was studied by Song *et al.* (2016) using piezoelectric materials. Nonlinear dynamic stability analysis of embedded temperature-dependent viscoelastic plates reinforced by single-walled carbon nanotubes (SWCNTs) was investigated by Kolahchi *et al.* (2016b). Zhang *et al.* (2017) investigated the impact responses of CNT reinforced functionally graded composite cylindrical shells.

For the seismic analysis of the structures, seismic response of buried pipes in longitudinal direction was studied by Nedjar *et al.* (2007). The effect of the variation of geotechnical properties of the surrounding soil on the stiffness, mass and damping of the soil was considered. The stress response of the piping system in the advanced power reactor 1400 (APR 1400) with a base isolation design subjected to seismic loading was addressed by Surh *et al.* (2015). Seismic responses of concrete pipes armed with Silica (SiO<sub>2</sub>) nanoparticles and concrete columns with nanofiber reinforced polymer layer were presented by Motezaker and Kolahchi (2017).

However, no researcher has examined the dynamic behavior of the smart nanocomposite pipes conveying fluid under earthquake load. This problem is very significant in the field of mechanical and civil engineering. So, in this research, for the first time, the seismic response of the

---

\*Corresponding author, Professor  
E-mail: r.kolahchi@gmail.com

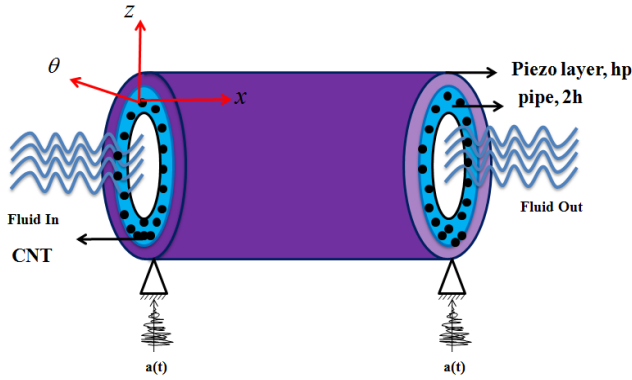


Fig. 1 A schematic figure of nanocomposite pipe covered by piezoelectric layer conveying fluid under seismic load

nanocomposite pipe covered with a piezoelectric layer and conveying fluid under earthquake load is investigated. Mori-Tanaka approach is applied to estimate the effective material properties of the nanocomposite and to consider the effect of the agglomeration. The governing equations of the structure are derived using energy method and according to Mindlin theory. Given that the extracted equations are nonlinear, harmonic differential quadrature method (HDQM) is employed to obtain the dynamic displacement of the structure caused by earthquake. In present paper, effect of various parameters like volume percent and agglomeration of carbon nanotubes (CNTs), external voltage applied to piezoelectric layer, geometrical parameters of pipe and boundary conditions on the dynamic displacement of the structure is studied.

## 2. Geometry of the problem

Fig. 1 shows a nanocomposite pipe with average radius  $R$ , thickness  $h$ , length  $L$  and density  $\rho_s$  in a cylindrical coordinate system  $(x, \theta, z)$ . The pipe is covered by a layer of piezoelectric with a thickness of  $h_p$  and density of  $\rho_p$  and conveying flow with density  $\rho_f$  and viscosity  $\mu_0$ . In all the following equations, the subscripts  $s$  and  $p$  stand for pipe and piezoelectric layer, respectively.

## 3. First order shear deformation theory (mindlin)

According to Mindlin theory, the displacement field is given as follows (Brush and Almoth 1975)

$$u(x, \theta, z, t) = u(x, \theta, t) + z\psi_x(x, \theta, t), \quad (1)$$

$$v(x, \theta, z, t) = v(x, \theta, t) + z\psi_\theta(x, \theta, t), \quad (2)$$

$$w(x, \theta, z, t) = w(x, \theta, t), \quad (2)$$

In which  $\psi_x$  and  $\psi_\theta$  are the angle of rotation around the  $x$  and  $\theta$  axes, respectively. Using above relations, the strain-displacement relations are obtained as follows

$$\varepsilon_{xx} = \frac{\partial u}{\partial x} + \frac{1}{2} \left( \frac{\partial w}{\partial x} \right)^2 + z \frac{\partial \psi_x}{\partial x}, \quad (4)$$

$$\varepsilon_{\theta\theta} = \frac{\partial v}{R\partial\theta} + \frac{w}{R} + \frac{1}{2} \left( \frac{\partial w}{R\partial\theta} \right)^2 + z \frac{\partial \psi_\theta}{R\partial\theta}, \quad (5)$$

$$\gamma_{x\theta} = \frac{\partial v}{\partial x} + \frac{\partial u}{R\partial\theta} + \frac{\partial w}{\partial x} \frac{\partial w}{R\partial\theta} + z \left( \frac{\partial \psi_x}{R\partial\theta} + \frac{\partial \psi_\theta}{\partial x} \right), \quad (6)$$

$$\gamma_{xz} = \frac{\partial w}{\partial x} + \psi_x, \quad (7)$$

$$\gamma_{\theta z} = \frac{\partial w}{R\partial\theta} - \frac{v}{R} + \psi_\theta, \quad (8)$$

## 4. Constitutive equations

### 4.1 Piezoelectric layer

The piezoelectric layer is made of polyvinylidene fluoride (PVDF) and is reinforced by CNTs. This material displays piezoelectric properties and is known as a smart material. In a piezoelectric material, stresses  $\sigma$  and strains  $\varepsilon$  tensors on the mechanical viewpoint, as well as flux density  $D$  and field strength  $E$  on the electrostatic viewpoint, can be arbitrarily combined as the following forms (Saviz 2015)

$$\begin{bmatrix} \sigma_{xx} \\ \sigma_{\theta\theta} \\ \sigma_{zz} \\ \tau_{\theta z} \\ \tau_{xz} \\ \tau_{x\theta} \end{bmatrix}_p = \begin{bmatrix} Q_{11} & Q_{12} & Q_{13} & 0 & 0 & 0 \\ Q_{12} & Q_{22} & Q_{23} & 0 & 0 & 0 \\ Q_{13} & Q_{23} & Q_{33} & 0 & 0 & 0 \\ 0 & 0 & 0 & Q_{44} & 0 & 0 \\ 0 & 0 & 0 & 0 & Q_{55} & 0 \\ 0 & 0 & 0 & 0 & 0 & Q_{66} \end{bmatrix} \begin{bmatrix} \varepsilon_{xx} \\ \varepsilon_{\theta\theta} \\ \varepsilon_{zz} \\ \gamma_{\theta z} \\ \gamma_{xz} \\ \gamma_{x\theta} \end{bmatrix} \quad (9)$$

$$\begin{bmatrix} 0 & 0 & e_{31} \\ 0 & 0 & e_{32} \\ 0 & 0 & e_{33} \\ 0 & e_{24} & 0 \\ e_{15} & 0 & 0 \\ 0 & 0 & 0 \end{bmatrix} \begin{Bmatrix} E_x \\ E_\theta \\ E_z \end{Bmatrix},$$

$$\begin{bmatrix} D_x \\ D_\theta \\ D_z \end{bmatrix} = \begin{bmatrix} 0 & 0 & 0 & 0 & e_{15} & 0 \\ 0 & 0 & 0 & e_{24} & 0 & 0 \\ e_{31} & e_{31} & e_{33} & 0 & 0 & 0 \end{bmatrix} \begin{Bmatrix} \varepsilon_{xx} \\ \varepsilon_{\theta\theta} \\ \varepsilon_{zz} \\ \gamma_{\theta z} \\ \gamma_{xz} \\ \gamma_{x\theta} \end{Bmatrix} \quad (10)$$

$$+ \begin{bmatrix} \varepsilon_{11} & 0 & 0 \\ 0 & \varepsilon_{22} & 0 \\ 0 & 0 & \varepsilon_{33} \end{bmatrix} \begin{Bmatrix} E_x \\ E_\theta \\ E_z \end{Bmatrix},$$

where  $Q_{ij}$ ,  $e_{ijk}$  and  $\varepsilon_{mk}$  are elastic, piezoelectric and dielectric constants, respectively. Also, electric field  $E_k$  in terms of electric potential  $\varphi$  is given as below (Kolahchi *et al.* 2016a)

$$E_k = -\nabla\phi. \tag{11}$$

In this paper, the electric potential distribution which satisfies the Maxwell equation is considered as follows

$$E_k = -\nabla\phi. \tag{12}$$

where  $V_0$  is the external electric voltage which is applied to the structure. So the electric field components may be obtained as

$$E_x = -\frac{\partial\phi}{\partial x} = -\sin\left(\frac{\pi(z-h)}{h_p}\right)\frac{\partial\phi}{\partial x}, \tag{13}$$

$$E_\theta = -\frac{\partial\phi}{R\partial\theta} = -\sin\left(\frac{\pi(z-h)}{h_p}\right)\frac{\partial\phi}{R\partial\theta}, \tag{14}$$

$$E_z = -\frac{\partial\phi}{\partial z} = -\frac{\pi}{h_p}\cos\left(\frac{\pi(z-h)}{h_p}\right)\phi - \frac{V_0}{h_p}. \tag{15}$$

Finally, by applying the classical theory, the coupled electro-mechanical relations of the piezoelectric layer can be rewritten as follows

$$\begin{bmatrix} \sigma_{xx} \\ \sigma_{\theta\theta} \\ \tau_{\theta z} \\ \tau_{xz} \\ \tau_{x\theta} \end{bmatrix}_p = \begin{bmatrix} Q_{11} & Q_{12} & 0 & 0 & 0 \\ Q_{12} & Q_{22} & 0 & 0 & 0 \\ 0 & 0 & Q_{44} & 0 & 0 \\ 0 & 0 & 0 & Q_{55} & 0 \\ 0 & 0 & 0 & 0 & Q_{66} \end{bmatrix} \begin{bmatrix} \varepsilon_{xx} \\ \varepsilon_{\theta\theta} \\ \gamma_{\theta z} \\ \gamma_{xz} \\ \gamma_{x\theta} \end{bmatrix} - \begin{bmatrix} 0 & 0 & e_{31} \\ 0 & 0 & e_{32} \\ 0 & e_{24} & 0 \\ e_{15} & 0 & 0 \\ 0 & 0 & 0 \end{bmatrix} \begin{bmatrix} E_x \\ E_\theta \\ E_z \end{bmatrix}, \tag{16}$$

$$\begin{bmatrix} D_x \\ D_\theta \\ D_z \end{bmatrix} = \begin{bmatrix} 0 & 0 & 0 & e_{15} & 0 \\ 0 & 0 & e_{24} & 0 & 0 \\ e_{31} & e_{32} & 0 & 0 & 0 \end{bmatrix} \begin{bmatrix} \varepsilon_{xx} \\ \varepsilon_{\theta\theta} \\ \gamma_{\theta z} \\ \gamma_{xz} \\ \gamma_{x\theta} \end{bmatrix} \tag{17}$$

$$+ \begin{bmatrix} \epsilon_{11} & 0 & 0 \\ 0 & \epsilon_{22} & 0 \\ 0 & 0 & \epsilon_{33} \end{bmatrix} \begin{bmatrix} E_x \\ E_\theta \\ E_z \end{bmatrix}.$$

### 4.2 Nanocomposite pipe

According to Hook's law, the constitutive equation of nanocomposite pipe is expressed as follows

$$\begin{bmatrix} \sigma_{xx} \\ \sigma_{\theta\theta} \\ \tau_{\theta z} \\ \tau_{xz} \\ \tau_{x\theta} \end{bmatrix}_s = \begin{bmatrix} C_{11} & C_{12} & 0 & 0 & 0 \\ C_{12} & C_{22} & 0 & 0 & 0 \\ 0 & 0 & C_{44} & 0 & 0 \\ 0 & 0 & 0 & C_{55} & 0 \\ 0 & 0 & 0 & 0 & C_{66} \end{bmatrix} \begin{bmatrix} \varepsilon_{xx} \\ \varepsilon_{\theta\theta} \\ \gamma_{\theta z} \\ \gamma_{xz} \\ \gamma_{x\theta} \end{bmatrix} \tag{18}$$

It should be noted that the effective material properties of the nanocomposite pipe  $C_{ij}$  are calculated based on Mori-

Tanaka approach and by considering the agglomeration effect which is addressed in Appendix A.

However, obtaining  $E$  and  $v$ , stiffness matrix of the structure can be calculated.

## 5. Energy method

One of the general and comprehensive ways to obtain the governing equations of the structure is equating the work done by external forces and the energy stored in the structure under load.

### 5.1 The strain energy

The strain energy of the structure is equals to sum of the strain energy which stored in the pipe and the piezoelectric layer and given as follows

$$U = \int_V \left[ (\sigma_{xx}\varepsilon_{xx} + \sigma_{\theta\theta}\varepsilon_{\theta\theta} + \tau_{x\theta}\gamma_{x\theta} + \tau_{xz}\gamma_{xz} + \tau_{z\theta}\gamma_{z\theta}) + (\sigma_{xx}\varepsilon_{xx} + \sigma_{\theta\theta}\varepsilon_{\theta\theta} + \tau_{x\theta}\gamma_{x\theta} + \tau_{xz}\gamma_{xz} + \tau_{z\theta}\gamma_{z\theta} - D_x E_x - D_\theta E_\theta - D_z E_z) \right] dV, \tag{19}$$

By substituting Eqs. (4)-(8) into Eq. (19) the strain energy stored in cylindrical shell can be expressed as below

$$\begin{aligned} U = & \frac{1}{2} \int_0^{2\pi} \int_0^L \left\{ (\sigma_{xx} + \sigma_{x\theta}) \left[ \frac{\partial u}{\partial x} + z \frac{\partial \psi_x}{\partial x} + \frac{1}{2} \left( \frac{\partial w}{\partial x} \right)^2 \right] + \right. \\ & (\sigma_{\theta\theta} + \sigma_{\theta\theta p}) \left[ \frac{1}{R} \left( w + \frac{\partial v}{\partial \theta} \right) + \frac{z}{R} \frac{\partial \psi_\theta}{\partial \theta} + \frac{1}{2} \left( \frac{\partial w}{R \partial \theta} \right)^2 \right] \\ & + (\tau_{x\theta} + \tau_{x\theta p}) \left( \frac{\partial v}{\partial x} + \frac{1}{R} \frac{\partial u}{\partial \theta} + z \frac{\partial \psi_\theta}{\partial x} + \frac{z}{R} \frac{\partial \psi_x}{\partial \theta} + \frac{\partial w}{R \partial \theta} \frac{\partial w}{\partial x} \right) \\ & + (\tau_{z\theta} + \tau_{z\theta p}) \left[ \frac{1}{R} \left( \frac{\partial w}{\partial \theta} - v \right) + \psi_\theta \right] + (\tau_{xz} + \tau_{xz p}) \left( \psi_x + \frac{\partial w}{\partial x} \right) \\ & \left. + D_x \left[ \sin\left(\frac{\pi(z-h)}{h_p}\right) \frac{\partial \phi}{\partial x} \right] + D_\theta \left[ \sin\left(\frac{\pi(z-h)}{h_p}\right) \frac{\partial \phi}{R \partial \theta} \right] + D_z \left[ \frac{\pi}{h_p} \cos\left(\frac{\pi(z-h)}{h_p}\right) \phi + \frac{V_0}{h_p} \right] \right\} R dx d\theta dz \end{aligned} \tag{20}$$

By introducing the stress resultants as below

$$\begin{Bmatrix} N_{xx} \\ N_{\theta\theta} \\ N_{x\theta} \end{Bmatrix} = \int_{-h}^h \begin{Bmatrix} \sigma_{xx} \\ \sigma_{\theta\theta} \\ \tau_{x\theta} \end{Bmatrix}_s dz + \int_h^{h+h_p} \begin{Bmatrix} \sigma_{xx} \\ \sigma_{\theta\theta} \\ \tau_{x\theta} \end{Bmatrix}_p dz, \tag{21}$$

$$\begin{Bmatrix} Q_x \\ Q_\theta \end{Bmatrix} = k \cdot \left( \int_{-h}^h \begin{Bmatrix} \tau_{xz} \\ \tau_{\theta z} \end{Bmatrix}_s dz + \int_h^{h+h_p} \begin{Bmatrix} \tau_{xz} \\ \tau_{\theta z} \end{Bmatrix}_p dz \right), \tag{22}$$

$$\begin{Bmatrix} M_{xx} \\ M_{\theta\theta} \\ M_{x\theta} \end{Bmatrix} = \int_{-h}^h \begin{Bmatrix} \sigma_{xx} \\ \sigma_{\theta\theta} \\ \tau_{x\theta} \end{Bmatrix}_s z dz + \int_h^{h+h_p} \begin{Bmatrix} \sigma_{xx} \\ \sigma_{\theta\theta} \\ \tau_{x\theta} \end{Bmatrix}_p z dz, \tag{23}$$

we have

$$\begin{aligned} U = & 0.5 \int \left[ N_{xx} \left( \frac{\partial u}{\partial x} + \frac{1}{2} \left( \frac{\partial w}{\partial x} \right)^2 \right) + N_{\theta\theta} \left( \frac{\partial v}{\partial x} + \frac{w}{R} + \frac{1}{2} \left( \frac{\partial w}{R \partial \theta} \right)^2 \right) \right. \\ & + Q_\theta \left( \frac{\partial w}{R \partial \theta} - v + \psi_\theta \right) + Q_x \left( \frac{\partial v}{\partial x} + \psi_x \right) + N_{x\theta} \left( \frac{\partial v}{\partial x} + \frac{\partial u}{R \partial \theta} + \frac{\partial w}{\partial x} \frac{\partial w}{R \partial \theta} \right) \\ & + M_{xx} \frac{\partial \psi_x}{\partial x} + M_{\theta\theta} \frac{\partial \psi_\theta}{R \partial \theta} + M_{x\theta} \left( \frac{\partial \psi_x}{R \partial \theta} + \frac{\partial \psi_\theta}{\partial x} \right) \Big] dA \\ & + 0.5 \int \left[ D_x \left( \sin\left(\frac{\pi(z-h)}{h_p}\right) \frac{\partial \phi}{\partial x} \right) + D_\theta \left( \sin\left(\frac{\pi(z-h)}{h_p}\right) \frac{\partial \phi}{R \partial \theta} \right) \right. \\ & \left. + D_z \left( \frac{\pi}{h_p} \cos\left(\frac{\pi(z-h)}{h_p}\right) \phi + \frac{V_0}{h_p} \right) \right] dz dA, \end{aligned} \tag{24}$$

where  $k'$  is the shear correction factor.

### 5.2 The kinetic energy

The kinetic energy of the structure can be described as follows

$$U = \frac{(\rho_s + \rho_p)}{2} \int (\dot{u}^2 + \dot{v}^2 + \dot{w}^2) dV \quad (25)$$

where  $\rho_s$  and  $\rho_p$  are the equivalent density of the nanocomposite pipe and piezoelectric layer, respectively. By substituting Eqs. (1)-(3) into Eq. (25), we have

$$K = \frac{(\rho_s + \rho_p)}{2} \int \left[ \left( \frac{\partial u}{\partial t} + z \frac{\partial \psi_x}{\partial t} \right)^2 + \left( \frac{\partial v}{\partial t} + z \frac{\partial \psi_\theta}{\partial t} \right)^2 + \left( \frac{\partial w}{\partial t} \right)^2 \right] dV. \quad (26)$$

By defining the following terms

$$\begin{cases} I_0 \\ I_1 \\ I_2 \end{cases} = \int_{-h}^h \begin{bmatrix} \rho \\ \rho z \\ \rho z^2 \end{bmatrix} dz + \int_h^{h+h_p} \begin{bmatrix} \rho \\ \rho z \\ \rho z^2 \end{bmatrix} dz, \quad (27)$$

Eq. (26) can be rewritten as below

$$\begin{aligned} K = 0.5 \int & \left[ I_0 \left( \left( \frac{\partial u}{\partial t} \right)^2 + \left( \frac{\partial v}{\partial t} \right)^2 + \left( \frac{\partial w}{\partial t} \right)^2 \right) \right. \\ & + 2I_1 \left( \frac{\partial u}{\partial t} \frac{\partial \psi_x}{\partial t} + \frac{\partial v}{\partial t} \frac{\partial \psi_\theta}{\partial t} \right) \\ & \left. + I_2 \left( \left( \frac{\partial \psi_x}{\partial t} \right)^2 + \left( \frac{\partial \psi_\theta}{\partial t} \right)^2 \right) \right] dA. \end{aligned} \quad (28)$$

### 5.3 The external work done due to the fluid flow

By assuming the Newtonian fluid, the governing equation of the fluid can be described by the well-known Navier-Stokes equation as below (Kolahchi and Monirbidgoli 2016)

$$\rho_f \frac{d\mathbf{V}}{dt} = -\nabla \mathbf{P} + \mu \nabla^2 \mathbf{V} + \mathbf{F}_{body}, \quad (29)$$

where  $V=(v_z, v_\theta, v_x)$  is the flow velocity vector in cylindrical coordinate system with components in longitudinal  $x$ , circumferential  $\theta$  and radial  $z$  directions. Also,  $P$ ,  $\mu$  and  $\rho_f$  are the pressure, the viscosity and the density of the fluid, respectively and  $F_{body}$  denotes the body forces. In Navier-Stokes equation, the total derivative operator with respect to  $t$  is

$$\frac{d}{dt} = \frac{\partial}{\partial t} + v_x \frac{\partial}{\partial x} + v_\theta \frac{\partial}{R \partial \theta} + v_z \frac{\partial}{\partial z}, \quad (30)$$

At the point of contact between the fluid and the core, the relative velocity and acceleration in the radial direction are equal. So

$$v_z = \frac{dw}{dt}, \quad (31)$$

By employing Eqs. (30) and (31) and substituting into Eq. (29), the pressure inside the pipe can be computed as

$$\begin{aligned} \frac{\partial p_z}{\partial z} = -\rho_f & \left( \frac{\partial^2 w}{\partial t^2} + 2v_x \frac{\partial^2 w}{\partial x \partial t} + v_x^2 \frac{\partial^2 w}{\partial x^2} \right) \\ & + \mu \left( \frac{\partial^3 w}{\partial x^2 \partial t} + \frac{\partial^3 w}{R^2 \partial \theta^2 \partial t} + v_x \left( \frac{\partial^3 w}{\partial x^3} + \frac{\partial^3 w}{R^2 \partial \theta^2 \partial x} \right) \right), \end{aligned} \quad (32)$$

By multiplying two sides of Eq. (32) in the inside area of the pipe ( $A$ ), the radial force in the pipe is calculated as below

$$\begin{aligned} F_{fluid} = A \frac{\partial p_z}{\partial z} = -\rho_f & \left( \frac{\partial^2 w}{\partial t^2} + 2v_x \frac{\partial^2 w}{\partial x \partial t} + v_x^2 \frac{\partial^2 w}{\partial x^2} \right) \\ & + \mu \left( \frac{\partial^3 w}{\partial x^2 \partial t} + \frac{\partial^3 w}{R^2 \partial \theta^2 \partial t} + v_x \left( \frac{\partial^3 w}{\partial x^3} + \frac{\partial^3 w}{R^2 \partial \theta^2 \partial x} \right) \right), \end{aligned} \quad (33)$$

Finally, the external work due to the pressure of the fluid may be obtained as follows

$$\begin{aligned} W_f = \int (F_{fluid}) w dA = \int & \left( -\rho_f \left( \frac{\partial^2 w}{\partial t^2} + 2v_x \frac{\partial^2 w}{\partial x \partial t} + v_x^2 \frac{\partial^2 w}{\partial x^2} \right) \right. \\ & \left. + \mu \left( \frac{\partial^3 w}{\partial x^2 \partial t} + \frac{\partial^3 w}{R^2 \partial \theta^2 \partial t} + v_x \left( \frac{\partial^3 w}{\partial x^3} + \frac{\partial^3 w}{R^2 \partial \theta^2 \partial x} \right) \right) \right) w dA, \end{aligned} \quad (34)$$

### 5.4 The external work done due to the earthquake

The external work due to the earthquake loads can be computed as below

$$W_s = \int \underbrace{(ma(t))}_{F_{Seismic}} w dA, \quad (35)$$

where  $m$  and  $a(t)$  are the mass of pipe and the applying acceleration from the Tabas earthquake (Peer site).

### 5.5 Hamilton's principle

The governing equations of the structure are derived using the Hamilton's principle which is considered as follows

$$\int_0^t (\delta U - \delta K - \delta W_f - \delta W_s) dt = 0. \quad (36)$$

Now, by applying the Hamilton's principle and after integration by part and some algebraic manipulation, six electro-mechanical equations of motion can be derived as follows

$$\delta u: \quad \frac{\partial N_{xx}}{\partial x} + \frac{\partial N_{x\theta}}{R \partial \theta} = I_0 \frac{\partial^2 u}{\partial t^2} + I_1 \frac{\partial^2 \psi_x}{\partial t^2}, \quad (37)$$

$$\delta v: \quad \frac{\partial N_{x\theta}}{\partial x} + \frac{\partial N_{\theta\theta}}{R \partial \theta} + \frac{Q_\theta}{R} = I_0 \frac{\partial^2 v}{\partial t^2} + I_1 \frac{\partial^2 \psi_\theta}{\partial t^2}, \quad (38)$$

$$\begin{aligned} \delta w: \quad & \frac{\partial Q_x}{\partial x} + \frac{\partial Q_\theta}{R \partial \theta} + \frac{\partial}{\partial x} \left( N_x^f \frac{\partial w}{\partial x} \right) \\ & + \frac{\partial}{R \partial \theta} \left( N_\theta^f \frac{\partial w}{R \partial \theta} \right) + F_{fluid} + F_{Seismic} = I_0 \frac{\partial^2 w}{\partial t^2}, \end{aligned} \quad (39)$$

$$\delta M_{\psi_x} : \frac{\partial M_{\psi_x}}{\partial x} + \frac{\partial M_{\psi_\theta}}{R\partial\theta} - Q_x = I_1 \frac{\partial^2 u}{\partial t^2} + I_2 \frac{\partial^2 \psi_x}{\partial t^2}, \quad (40)$$

$$\delta M_{\psi_\theta} : \frac{\partial M_{\psi_\theta}}{\partial x} + \frac{\partial M_{\theta\theta}}{R\partial\theta} - Q_\theta = I_1 \frac{\partial^2 v}{\partial t^2} + I_2 \frac{\partial^2 \psi_\theta}{\partial t^2}, \quad (41)$$

$$\delta\phi : \int_{h_c}^{h_s} \left( \left( \sin\left(\frac{\pi(z-h)}{h_p}\right) \frac{\partial D_x}{\partial x} \right) + \left( \sin\left(\frac{\pi(z-h)}{h_p}\right) \frac{\partial D_\theta}{R\partial\theta} \right) + D_x \left( \frac{\pi}{h_p} \cos\left(\frac{\pi(z-h)}{h_p}\right) \right) \right) dz. \quad (42)$$

Now, by substituting Eqs. (B1)-(B8) into the equations of motion (Eqs. (37)-(42)) we have

$$\begin{aligned} & A_{11} \left( \frac{\partial^2 u}{\partial x^2} + \frac{\partial w}{\partial x} \frac{\partial^2 w}{\partial x^2} \right) + B_{11} \left( \frac{\partial^2 \psi_x}{\partial x^2} \right) \\ & + A_{12} \left( \frac{\partial^2 v}{R\partial x \partial \theta} + \frac{\partial w}{R\partial x} + \frac{\partial w}{R\partial\theta} \frac{\partial^2 w}{R\partial x \partial \theta} \right) \\ & + B_{12} \left( \frac{\partial^2 \psi_\theta}{R^2 \partial x \partial \theta} \right) + E_{31} \frac{\partial \phi}{\partial x} \\ & + \frac{A_{66}}{R} \left( \frac{\partial^2 u}{R\partial\theta^2} + \frac{\partial^2 v}{\partial x \partial \theta} + \frac{\partial^2 w}{\partial x \partial \theta} \frac{\partial w}{R\partial\theta} + \frac{\partial w}{\partial x} \frac{\partial^2 w}{R\partial\theta^2} \right) \\ & + \frac{B_{66}}{R} \left( \frac{\partial^2 \psi_x}{R\partial\theta^2} + \frac{\partial^2 \psi_\theta}{\partial x \partial \theta} \right) = I_0 \frac{\partial^2 u}{\partial t^2} + I_1 \frac{\partial^2 \psi_x}{\partial t^2}, \end{aligned} \quad (43)$$

$$\begin{aligned} & A_{66} \left( \frac{\partial^2 u}{R\partial\theta \partial x} + \frac{\partial^2 v}{\partial x^2} + \frac{\partial^2 w}{\partial x^2} \frac{\partial w}{R\partial\theta} + \frac{\partial w}{\partial x} \frac{\partial^2 w}{R\partial\theta \partial x} \right) \\ & + B_{66} \left( \frac{\partial^2 \psi_x}{R\partial\theta \partial x} + \frac{\partial^2 \psi_\theta}{\partial x^2} \right) + \frac{A_{12}}{R} \left( \frac{\partial^2 u}{\partial x \partial \theta} + \frac{\partial w}{\partial x} \frac{\partial^2 w}{\partial x \partial \theta} \right) \\ & + \frac{B_{12}}{R} \left( \frac{\partial^2 \psi_x}{\partial x \partial \theta} \right) + \frac{A_{22}}{R} \left( \frac{\partial^2 v}{R\partial\theta^2} + \frac{\partial w}{R\partial\theta} + \frac{\partial w}{R\partial\theta} \frac{\partial^2 w}{R\partial\theta^2} \right) \\ & + \frac{B_{22}}{R} \left( \frac{\partial^2 \psi_\theta}{R^2 \partial \theta^2} \right) + E_{32} \frac{\partial \phi}{R\partial\theta} = I_0 \frac{\partial^2 v}{\partial t^2} + I_1 \frac{\partial^2 \psi_\theta}{\partial t^2}, \end{aligned} \quad (44)$$

$$\begin{aligned} & A_{55} \left( \frac{\partial^3 w}{\partial x^2} + \frac{\partial \psi_x}{\partial x} \right) - E_{15} \frac{\partial^2 \phi}{\partial x^2} \\ & + \frac{A_{44}}{R} \left( \frac{\partial^3 w}{R\partial\theta^2} - \frac{\partial v}{R\partial\theta} + \frac{\partial \psi_\theta}{\partial \theta} \right) - E_{24} \frac{\partial^2 \phi}{R^2 \partial \theta^2} \\ & - \rho_f K_p \left( \frac{\partial^2 w}{\partial t^2} + 2v_x \frac{\partial^2 w}{\partial x \partial t} + v_x^2 \frac{\partial^2 w}{\partial x^2} \right) \\ & + \frac{\partial}{R\partial\theta} \left( N_\theta^f \frac{\partial w}{R\partial\theta} \right) + \frac{\partial}{\partial x} \left( N_x^f \frac{\partial w}{\partial x} \right) + F_{Seismic} \\ & + \mu \left( \frac{\partial^3 w}{\partial x^2 \partial t} + \frac{\partial^3 w}{R^2 \partial \theta^2 \partial t} + v_x \left( \frac{\partial^3 w}{\partial x^3} + \frac{\partial^3 w}{R^2 \partial \theta^2 \partial x} \right) \right) = I_0 \frac{\partial^2 w}{\partial t^2}, \end{aligned} \quad (45)$$

$$\begin{aligned} & B_{11} \left( \frac{\partial^2 u}{\partial x^2} + \frac{\partial w}{\partial x} \frac{\partial^2 w}{\partial x^2} \right) + D_{11} \left( \frac{\partial^2 \psi_x}{\partial x^2} \right) \\ & + B_{12} \left( \frac{\partial^2 v}{R\partial\theta \partial x} + \frac{\partial w}{R\partial x} + \frac{\partial^2 w}{R\partial\theta \partial x} \right) \\ & + D_{12} \left( \frac{\partial^2 \psi_\theta}{R\partial\theta \partial x} \right) + F_{31} \frac{\partial \phi}{\partial x} \\ & + \frac{B_{66}}{R} \left( \frac{\partial^2 u}{R\partial\theta^2} + \frac{\partial^2 v}{\partial x \partial \theta} + \frac{\partial^2 w}{\partial x \partial \theta} \frac{\partial w}{R\partial\theta} + \frac{\partial w}{\partial x} \frac{\partial^2 w}{R\partial\theta^2} \right) \\ & + \frac{D_{66}}{R} \left( \frac{\partial^2 \psi_x}{R\partial\theta^2} + \frac{\partial^2 \psi_\theta}{\partial x \partial \theta} \right) - A_{55} \left( \frac{\partial w}{\partial x} + \psi_x \right) \\ & + E_{15} \frac{\partial \phi}{\partial x} = I_1 \frac{\partial^2 u}{\partial t^2} + I_2 \frac{\partial^2 \psi_x}{\partial t^2}, \end{aligned} \quad (46)$$

$$\begin{aligned} & B_{66} \left( \frac{\partial^2 u}{R\partial\theta \partial x} + \frac{\partial^2 v}{\partial x^2} + \frac{\partial^2 w}{\partial x^2} \frac{\partial w}{R\partial\theta} + \frac{\partial w}{\partial x} \frac{\partial^2 w}{R\partial\theta \partial x} \right) \\ & + D_{66} \left( \frac{\partial^2 \psi_x}{R\partial\theta \partial x} + \frac{\partial^2 \psi_\theta}{\partial x^2} \right) + \frac{B_{12}}{R} \left( \frac{\partial^2 u}{\partial x \partial \theta} + \frac{\partial w}{\partial x} \frac{\partial^2 w}{\partial x \partial \theta} \right) \\ & + \frac{D_{12}}{R} \left( \frac{\partial^2 \psi_x}{\partial x \partial \theta} \right) + \frac{B_{22}}{R} \left( \frac{\partial^2 v}{R\partial\theta^2} + \frac{\partial w}{R\partial\theta} + \frac{\partial w}{R\partial\theta} \frac{\partial^2 w}{R\partial\theta^2} \right) \\ & + \frac{D_{22}}{R} \left( \frac{\partial^2 \psi_\theta}{R^2 \partial \theta^2} \right) + F_{32} \frac{\partial \phi}{R\partial\theta} - A_{44} \left( \frac{\partial w}{R\partial\theta} - \frac{v}{R} + \psi_\theta \right) \\ & + E_{24} \frac{\partial \phi}{R\partial\theta} = I_1 \frac{\partial^2 v}{\partial t^2} + I_2 \frac{\partial^2 \psi_\theta}{\partial t^2}, \end{aligned} \quad (47)$$

$$\begin{aligned} & \frac{2e_{15}h}{\pi} \frac{\partial w}{\partial x} + \frac{2e_{15}h}{\pi} \psi_x + \frac{\epsilon_{11}h}{2} \frac{\partial \phi}{\partial x} + \frac{2e_{24}h}{\pi} \frac{\partial w}{R\partial\theta} \\ & - \frac{2e_{24}h}{\pi} \frac{v}{R} + \frac{2e_{24}h}{\pi} \psi_\theta + \frac{\epsilon_{22}h}{2} \frac{\partial \phi}{R\partial\theta} \\ & - \frac{2he_{32}}{\pi} \frac{\partial^2 w}{R^2 \partial \theta^2} + \frac{2h}{\pi} e_{31} \frac{\partial \psi_x}{\partial x} - \frac{\pi^2 \epsilon_{33}}{2h} \phi = 0. \end{aligned} \quad (48)$$

Also, the boundary conditions are considered as below

• Clamped-Clamped supported

$$x = 0, L \Rightarrow u = v = w = \psi_x = \psi_\theta = 0, \quad (49)$$

• Simply-Simply supported

$$x = 0, L \Rightarrow u = v = w = \psi_\theta = M_{xx} = 0, \quad (50)$$

• Clamped-Simply supported

$$\begin{aligned} x = 0 & \Rightarrow u = v = w = \psi_x = \psi_\theta = 0, \\ x = L & \Rightarrow u = v = w = \psi_x = M_{xx} = 0. \end{aligned} \quad (51)$$

Given that the governing equations are nonlinear, so HDQ method along with Newmark method is applied to achieve results with higher accuracy.

### 6. HDQ method

HDQM is one of the numerical methods in which the governing differential equations turn into a set of first order algebraic equations by applying the weighting coefficients. So that, at a given discrete point, a derivative of a function with respect to a spatial variable will be expressed as a weighted linear sum of the function values at all discrete points chosen in the solution domain of that variable and in the direction of the axes of coordinate system (Civalek 2004I, Jafarian Arani and Kolahchi 2016, Safari Bilouei *et al.* 2016). In these methods, the one-dimensional and two-dimensional derivative of the function may be defined as follows

$$\frac{d^n f_x(x_i, \theta_j)}{dx^n} = \sum_{k=1}^{N_x} A_{ik}^{(n)} f(x_k, \theta_j) \quad n = 1, \dots, N_x - 1. \quad (52)$$

$$\frac{d^m f_y(x_i, \theta_j)}{d\theta^m} = \sum_{l=1}^{N_\theta} B_{jl}^{(m)} f(x_i, \theta_l) \quad m = 1, \dots, N_\theta - 1. \quad (53)$$

$$\frac{d^{n+m} f_{xy}(x_i, \theta_j)}{dx^n d\theta^m} = \sum_{k=1}^{N_x} \sum_{l=1}^{N_\theta} A_{ik}^{(n)} B_{jl}^{(m)} f(x_k, \theta_l). \quad (54)$$

So, it is apparent that the two most important factors in determining the accuracy of HDQ, are the selection of sampling grid points and weighting coefficients. For choosing sampling grid points, the Chebyshev polynomials are used as follows

$$X_i = \frac{L}{2} \left[ 1 - \cos\left(\frac{i-1}{N_x-1}\pi\right) \right] \quad i = 1, \dots, N_x \quad (55)$$

$$\theta_i = \frac{2\pi}{2} \left[ 1 - \cos\left(\frac{i-1}{N_\theta-1}\pi\right) \right] \quad i = 1, \dots, N_\theta \quad (56)$$

The weighting coefficients can be obtained by the following simple algebraic relations

$$A_{ij}^{(1)} = \begin{cases} \frac{(\pi/2)M(x_i)}{M(x_j)\sin[(x_i-x_j)/2]\pi} & \text{for } i \neq j, \quad i, j=1,2,\dots,N_x, \\ -\sum_{\substack{j=1 \\ i \neq j}}^{N_x} A_{ij}^{(1)} & \text{for } i = j, \quad i, j=1,2,\dots,N_x \end{cases} \quad (57)$$

$$B_{ij}^{(1)} = \begin{cases} \frac{(\pi/2)P(\theta_i)}{P(\theta_j)\sin[(\theta_i-\theta_j)]\pi} & \text{for } i \neq j, \quad i, j=1,2,\dots,N_\theta, \\ -\sum_{\substack{j=1 \\ i \neq j}}^{N_\theta} B_{ij}^{(1)} & \text{for } i = j, \quad i, j=1,2,\dots,N_\theta \end{cases} \quad (58)$$

in which

$$M(x_i) = \prod_{\substack{j=1 \\ j \neq i}}^{N_x} \sin\left(\frac{(x_i-x_j)\pi}{2}\right) \quad (59)$$

$$P(\theta_i) = \prod_{\substack{j=1 \\ j \neq i}}^{N_\theta} \sin\left(\frac{(\theta_i-\theta_j)\pi}{2}\right) \quad (60)$$

and for higher-order derivatives we have

$$A_{ij}^{(n)} = n \left( A_{ii}^{(n-1)} A_{ij}^{(1)} - \pi c t g\left(\frac{x_i-x_j}{2}\right) \pi \right) \quad (61)$$

$$B_{ij}^{(m)} = m \left( B_{ii}^{(m-1)} B_{ij}^{(1)} - \pi c t g\left(\frac{\theta_i-\theta_j}{2}\right) \pi \right) \quad (62)$$

Considering  $N_x=N_\theta=N$  and substituting above equations into the motion equations (Eqs. (43)-(48)), the motion equations and boundary conditions may be rewritten in the matrix form as below

$$\left[ \begin{matrix} [K_L + K_{NL}] \\ [K_L + K_{NL}] \end{matrix} \right]_{6N^2 \times 6N^2} \begin{Bmatrix} \{d_b\} \\ \{d_d\} \end{Bmatrix}_{6N^2 \times 1} + [C]_{6N^2 \times 6N^2} \begin{Bmatrix} \{\dot{d}_b\} \\ \{\dot{d}_d\} \end{Bmatrix}_{6N^2 \times 1} + [M]_{6N^2 \times 6N^2} \begin{Bmatrix} \{\ddot{d}_b\} \\ \{\ddot{d}_d\} \end{Bmatrix}_{6N^2 \times 1} = \begin{Bmatrix} \{0\} \\ -m\ddot{a}(t) \end{Bmatrix}_{6N^2 \times 1}, \quad (63)$$

where  $[K_L]$ ,  $[K_{NL}]$ ,  $[C]$  and  $[M]$  denote linear part of the stiffness matrix, nonlinear part of the stiffness matrix, the

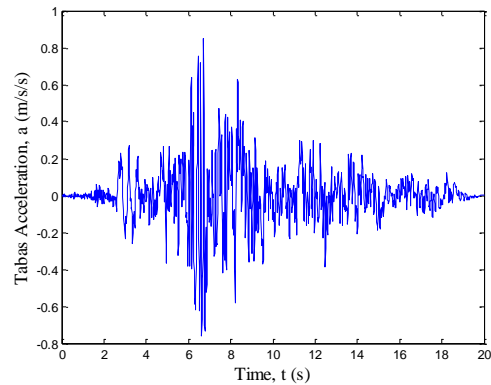


Fig. 2 Acceleration history of Tabas earthquake

damping matrix and the mass matrix, respectively. Also,  $\{db\} = \{u_1, v_1, w_1, w_2, \psi_{x1}, \psi_{\theta1}, \phi_1, u_N, v_N, w_{N-1}, w_N, \psi_{xN}, \psi_{\theta N}, \phi_N\}$  and  $\{dd\} = \{u_{2:N-1}, v_{2:N-1}, w_{3:N-2}, \psi_{x2:N-1}, \phi_{2:N-1}\}$  represent boundary and domain points, respectively.

### 7. Newmark method

In this section, Newmark method (Simsek 2010, Motezaker and Kolahchi 2017) is applied in the time domain to obtain the time response of the structure under the earthquake loads. Based on this method, Eq. (56) can be written in the general form as below

$$K^*(d_{i+1}) = Q_{i+1}, \quad (64)$$

where subscript  $i+1$  indicates the time  $t=t_{i+1}$ ,  $K^*(d_{i+1})$  and  $Q_{i+1}$  are the effective stiffness matrix and the effective load vector which can be considered as

$$K^*(d_{i+1}) = K_L + K_{NL}(d_{i+1}) + \alpha_0 M + \alpha_1 C, \quad (65)$$

$$Q_{i+1}^* = Q_{i+1} + M(\alpha_0 d_i + \alpha_2 \dot{d}_i + \alpha_3 \ddot{d}_i) + C(\alpha_1 d_i + \alpha_4 \dot{d}_i + \alpha_5 \ddot{d}_i), \quad (66)$$

where

$$\begin{aligned} \alpha_0 &= \frac{1}{\chi \Delta t^2}, & \alpha_1 &= \frac{\gamma}{\chi \Delta t}, & \alpha_2 &= \frac{1}{\chi \Delta t}, \\ \alpha_3 &= \frac{1}{2\chi} - 1, & \alpha_4 &= \frac{\gamma}{\chi} - 1, & \alpha_5 &= \frac{\Delta t}{2} \left( \frac{\gamma}{\chi} - 2 \right), \\ \alpha_6 &= \Delta t (1 - \gamma), & \alpha_7 &= \Delta t \gamma, \end{aligned} \quad (67)$$

in which  $\gamma=0.5$  and  $\chi=0.25$ . Based on the iteration method, Eq. (64) is solved at any time step and modified velocity and acceleration vectors are calculated as follows

$$\ddot{d}_{i+1} = \alpha_0 (d_{i+1} - d_i) - \alpha_2 \dot{d}_i - \alpha_3 \ddot{d}_i, \quad (68)$$

$$\dot{d}_{i+1} = \dot{d}_i + \alpha_6 \ddot{d}_i + \alpha_7 \ddot{d}_{i+1}, \quad (69)$$

Then for the next time step, the modified velocity and acceleration vectors in Eqs. (68) and (69) are employed and all these procedures mentioned above are repeated.

Table 1 Material property of PE, PVDF and CNT

| PVDF                                              | CNT                            | PE                           |
|---------------------------------------------------|--------------------------------|------------------------------|
| $C_{11} = 238.24(\text{GPa})$                     | $E = 1(\text{TPa})$            | $E = 125(\text{GPa})$        |
| $C_{22} = 23.6(\text{GPa})$                       | $\nu = 0.34$                   | $\nu = 0.30$                 |
| $C_{12} = 3.98(\text{GPa})$                       | $\rho = 1.4(\text{gr / cm}^3)$ | $\rho = 1.45(\text{kg/m}^3)$ |
| $C_{66} = 6.43(\text{GPa})$                       |                                |                              |
| $e_{11} = -0.135(\text{C/m}^2)$                   |                                |                              |
| $e_{12} = -0.145(\text{C/m}^2)$                   |                                |                              |
| $\epsilon = 1.1068 \times 10^{-8} (\text{F/m})$   |                                |                              |
| $\alpha_x = 7.1 \times 10^{-5} (1/\text{K})$      |                                |                              |
| $\alpha_\theta = 7.1 \times 10^{-5} (1/\text{K})$ |                                |                              |

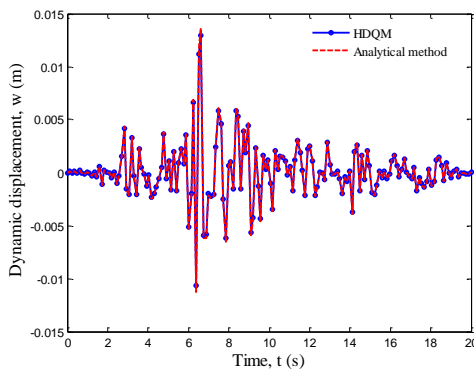


Fig. 3 Comparison of analytical and numerical results

## 8. Numerical results

In this section, the numerical results for the dynamic response of the pipeline which is reinforced by CNTs and covered with piezoelectric layer under the earthquake loads are examined. For this purpose, a polyethylene pipe of length  $L=2$  m,  $R=20$  in and thickness  $h=1$  in is considered. The pipe is covered with a piezoelectric layer of PVDF with the thickness  $h_p=5$  mm and conveying a fluid flow of velocity  $v_x=40$  ft/s and viscosity  $\mu=63.6$  Pa.s. The elastic and piezoelectric properties of these materials are given in Table 1 (Kolahch *et al.* 2016a).

It is worth mentioning that the acceleration of the earthquake is considered according to Bam earthquake that the distribution of acceleration in 20 seconds is shown in Fig. 2.

### 8.1 Verification

Since this research has been defined for the first time in the world, there is not any reference to validate the obtained results. Therefore, it has been tried to examine the results without considering the nonlinear terms of the governing equations and by comparing the linear dynamic response of the structure which obtained by two various solution methods. For the analytical method, the Navier method is used with the following relations for SS pipe

$$u(x, \theta, z) = u_0(t) \sin\left(\frac{m\pi x}{a}\right) \cos(n\theta), \quad (70)$$

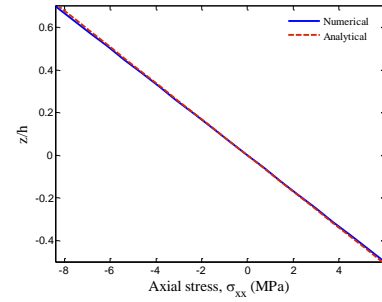


Fig. 4 Distribution of axial stress across the thickness direction

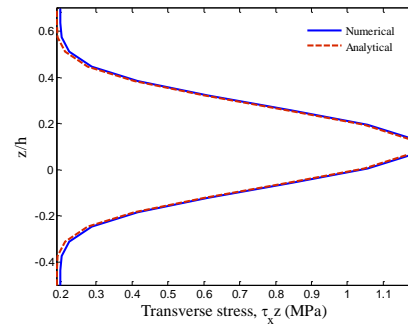


Fig. 5 Distribution of transverse stress across the thickness direction

$$v(x, \theta, z) = v_0(t) \cos\left(\frac{m\pi x}{a}\right) \sin(n\theta), \quad (71)$$

$$w(x, \theta, z) = v_0(t) \sin\left(\frac{m\pi x}{a}\right) \sin(n\theta), \quad (72)$$

$$\psi_x(x, \theta, z) = \psi_{x0}(t) \sin\left(\frac{m\pi x}{a}\right) \cos(n\theta), \quad (73)$$

$$\psi_\theta(x, \theta, z) = \psi_{\theta0}(t) \cos\left(\frac{m\pi x}{a}\right) \sin(n\theta), \quad (74)$$

$$\phi(x, \theta, z) = \phi_0(t) \sin\left(\frac{m\pi x}{a}\right) \sin(n\theta), \quad (75)$$

Substituting Eqs. (70)-(75) into Eqs. (43)-(48) yields

$$([K_L]\{d\} + [C]\{\dot{d}\} + [M]\{\ddot{d}\}) = \{-ma(t)\}, \quad (76)$$

Finally, using Newmark, the dynamic response of the structure can be obtained. The results of the analytical and numerical (HDQ) methods are depicted in Fig. 3. As it can be seen, the difference between the analytical method and HDQ method is negligible and so, the obtained results are accurate and acceptable.

In another comparison, the maximum deflection and stresses of the structure are reported in Table 2. In addition, the distributions of axial and transverse stresses are shown in Figs. 4 and 5 for a special time. As can be seen, the numerical and analytical results match with each others.

Table 2 Comparison of analytical and numerical methods for maximum deflection and stresses of the pipe

| $c_r$      | $w(m)$  | $\sigma_{xx}$ (MPa) | $\sigma_{\theta\theta}$ (MPa) | $\tau_{x\theta}$ (MPa) | $\tau_{xz}$ (MPa) | $\tau_{\theta z}$ (MPa) |
|------------|---------|---------------------|-------------------------------|------------------------|-------------------|-------------------------|
| Numerical  | 0.02521 | 8.4476              | 6.2018                        | 4.4405                 | 1.1125            | 0.8091                  |
| Analytical | 0.02520 | 8.4475              | 6.2016                        | 4.4404                 | 1.1122            | 0.8089                  |

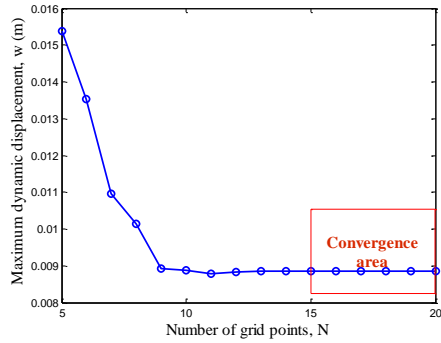


Fig. 6 Convergence and accuracy of HDQM

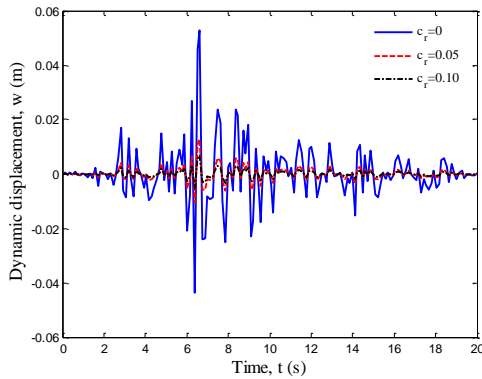


Fig. 7 The effect of CNTs volume percent on the dynamic deflection of the structure

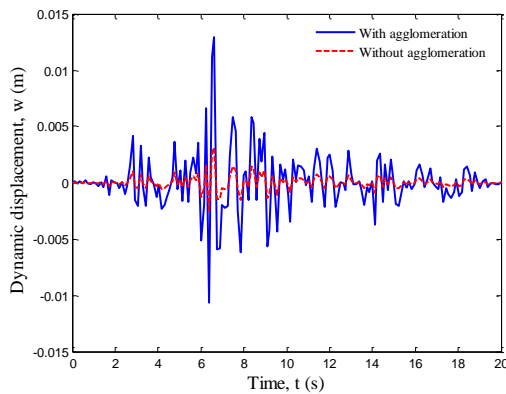


Fig. 8 The effect of CNTs agglomeration on the dynamic deflection of the structure

8.2 The convergence of numerical method

The convergence of HDQ method in evaluating the maximum deflection of the structure versus number of grid points is illustrated in Fig. 6. As it can be seen, with increasing the number of grid points, the maximum deflection of the structure decreases so far as, at  $N=15$  the

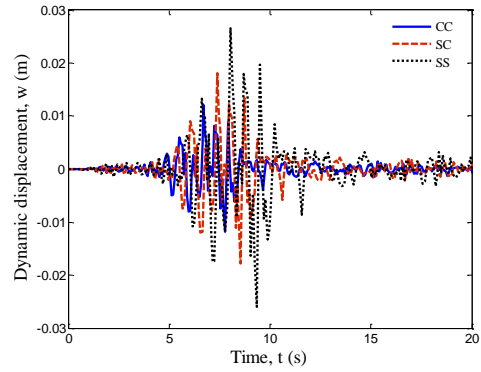


Fig. 9 The effect of boundary conditions on the dynamic deflection of the structure

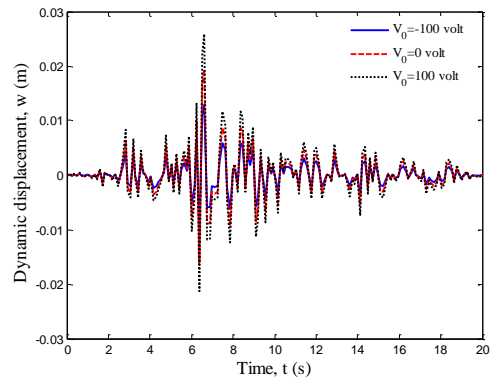


Fig. 10 The effect of applied external voltage on the dynamic deflection of the structure

deflection converges. So, the results presented below are based on the number of grid points 15 for DQ solution method.

8.3 Effect of various parameters

Fig. 7 shows the effect of CNTs volume percent on the dynamic deflection of the structure versus time. The changes of the deflection are shown for  $c_r=0$ ,  $c_r=0.05$  and  $c_r=0.10$ . It is apparent that with increasing of CNTs volume percent, the dynamic deflection of the system reduces because the stiffness of the structure increases.

The agglomeration effect of CNTs on the dynamic deflection of the structure versus time is indicated by Fig. 8.

It can be found that considering the agglomeration decreases the stiffness of the structure and as a result, the displacement of the structure increases. Given that during the process of nanocomposite manufacturing, the uniform distribution for CNTs in the polymer matrix is impossible, so the results of this figure can be very significant. So it can be concluded that about CNTs reinforced pipes, as the agglomeration in various regions decreases, the displacement of the structure decreases.

Fig. 9 illustrates the effect of various boundary conditions on the dynamic displacement of the structure versus time. It is found that, the boundary conditions have a significant effect on the dynamic displacement of the system so that the pipe with clamped-clamped boundary condition has the lowest deflection. It is predictable,

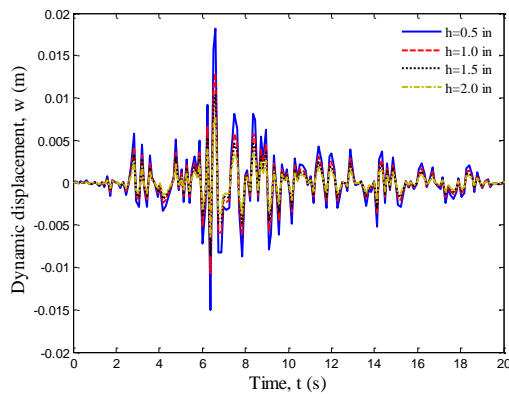


Fig. 11 The effect of pipe thickness on the dynamic deflection of the structure

because the constraint of clamped boundary condition is stronger than the other ones and consequently the structure is stiffer. Also, among the mentioned boundary conditions Eqs. (85)-(87), simply-simply boundary condition denotes the most dynamic displacement.

Fig. 10 indicates the effect of the applied external voltage to the piezoelectric layer on the dynamic deflection versus time. It can be observed that by applying the positive voltage to the structure, dynamic deflection of system increases and it is because of the tensile force which exerted to the structure and makes the structure softer. Applying the external negative voltage has a reverse effect and leads to compressive force in the structure and decreases the dynamic deflection of the system. Thus, the external voltage is an important parameter to control the dynamic behavior of the structure.

Effect of pipe thickness on the deflection behavior versus time is shown in Fig. 11. It can be seen that by increasing the thickness of the pipe, the stiffness of the structure increases and so the dynamic deflection of the system decreases.

## 9. Conclusions

In this study, the electro-mechanical dynamic response of a nanocomposite polyethylene pipe covered with a piezoelectric layer under the earthquake load was examined using HDQM and Newmark method. The pipe conveying viscous fluid flow was reinforced by CNTs. For modeling and determining the mechanical properties of nanocomposite, the Mori-Tanaka approach was used by considering the agglomeration effect. By applying the nonlinear strain-displacement relations, Mindlin theory and the stress-strain relations, the general energy formulation was obtained and by employing Hamilton's principle or virtual work method, the equations of motion were obtained. The aim of this research was to investigate the effects of volume percent of CNTs, the agglomeration of CNTs, boundary conditions, geometrical parameters of pipe and the external applied voltage to the piezoelectric layer on the dynamic displacement of the structure for the Bam earthquake features. According to the plotted figures, the

following results were obtained:

1. The difference between HDQM and the analytical method was negligible and it shows the validity of the results of the present study.

2. With increasing the volume percent of CNTs, the dynamic deflection of the system decreases that it was because of the increasing of the stiffness of the structure.

3. Considering the agglomeration effect of CNTs, decreases the stiffness of the structure while increases the displacement of that.

4. Boundary conditions have a remarkable effect on the dynamic displacement of the system so that the lowest dynamic displacement belongs to the pipe with clamped-clamped boundary condition.

5. By applying the positive voltage to the structure, the dynamic deflection of the system increases. However, applying the external negative voltage has a reverse effect and decreases the dynamic deflection of the system by exerting the compressive forces.

6. With increasing the thickness of the pipe, the stiffness of the structure increases and therefore the dynamic deflection of the system decreases.

## References

- Amabili, M. (2003), "A comparison of shell theories for large-amplitude vibrations of circular cylindrical shells: Lagrangian approach", *J. Sound Vibr.*, **264**(5), 1091-1125.
- Amabili, M. and Garziera, R. (2002), "Vibrations of circular cylindrical shells with nonuniform constraints, elastic bed and added mass. Part II: Shells containing or immersed in axial flow", *J. Fluid. Struct.*, **16**(1), 31-51.
- Brush, O. and Almorh, B. (1975), *Buckling of Bars, Plates and Shells*, Mc-Graw Hill.
- Civalek, O. (2004), "Application of differential quadrature (DQ) and harmonic differential quadrature (HDQ) for buckling analysis of thin isotropic plates and elastic columns", *Eng. Struct.*, **26**(2), 171-186.
- Jafarian Arani, A. and Kolahchi, R. (2016), "Buckling analysis of embedded concrete columns armed with carbon nanotubes", *Comput. Concrete*, **17**(5), 567-578.
- Kolahchi, R. and Moniribidgoli, A.M. (2016), "Size-dependent sinusoidal beam model for dynamic instability of single-walled carbon nanotubes", *Appl. Math. Mech.*, **37**(2), 265-274.
- Kolahchi, R., Hosseini, H. and Esmailpour, M. (2016a), "Differential cubature and quadrature-Bolotin methods for dynamic stability of embedded piezoelectric nanoplates based on visco-nonlocal-piezoelasticity theories", *Compos. Struct.*, **157**, 174-186.
- Kolahchi, R., Safari, M. and Esmailpour, M. (2016b), "Dynamic stability analysis of temperature-dependent functionally graded CNT-reinforced visco-plates resting on orthotropic elastomeric medium", *Compos. Struct.*, **150**, 255-265.
- Maturi, D.A., Ferreira, A.J.M., Zenkour, A.M. and Mashat, D.S. (2015), "Analysis of three-layer composite shells by a new layerwise theory and radial basis functions collocation, accounting for through-the-thickness deformations", *Mech. Adv. Mater. Struct.*, **22**(9), 722-730.
- Mori, T. and Tanaka, K. (1973), "Average stress in matrix and average elastic energy of materials with misfitting inclusions", *Acta Metall. Mater.*, **21**(5), 571-574.
- Motezaker, M. and Kolahchi, R. (2017), "Seismic response of concrete columns with nanofiber reinforced polymer layer",

- Comput. Concrete*, In Press.
- Motezaker, M. and Kolahchi, R. (2017), "Seismic response of SiO<sub>2</sub> nanoparticles-reinforced concrete pipes based on DQ and newmark methods", *Comput. Concrete*, **19**(6), 751-759.
- Nedjar, D., Hamane, M., Bensafi, M., Elachachi, S.M. and Breyse, D. (2007), "Seismic response analysis of pipes by a probabilistic approach", *Soil Dyn. Earthq. Eng.*, **27**(2), 111-115.
- Païdoussis, M.P. (2003), *Fluid-Structure Interactions: Slender Structures and Axial Flow*, Elsevier Academic Press, London, U.K.
- Païdoussis, M.P. and Denise, J.P. (1972), "Flutter of thin cylindrical shells conveying fluid", *J. Sound Vibr.*, **20**(1), 9-26.
- Safari Bilouei, B., Kolahchi, R. and Rabani Bidgoli, M. (2016), "Buckling of concrete columns retrofitted with nano-fiber reinforced polymer (NFRP)", *Comput. Concrete*, **18**(5), 1053-1063.
- Saviz, M.R. (2015), "Dynamic analysis of a laminated cylindrical shell with piezoelectric layer and clamped boundary condition", *Finit. Elem. Anal. Des.*, **104**, 1-15.
- Shi, D.L. and Feng, X. (2004), "The effect of nanotube waviness and agglomeration on the elastic property of carbon nanotube-reinforced composites", *J. Eng. Mater. Technol.*, **126**(3), 250-270.
- Simsek, M. (2010), "Non-linear vibration analysis of a functionally graded Timoshenko beam under action of a moving harmonic load", *Compos. Struct.*, **92**(10), 2532-2546.
- Song, Z.G., Zhang, L.W. and Liew, K.M. (2016), "Active vibration control of CNT-reinforced composite cylindrical shells via piezoelectric patches", *Compos. Struct.*, **158**, 92-100.
- Surh, H.B., Ryu, T.Y., Park, J.S., Ahn, E.W. and Kim, M.K. (2015), "Seismic response analysis of a piping system subjected to multiple support excitations in a base isolated NPP building", *Nucl. Eng. Des.*, **292**, 283-295.
- Weaver, D.S. and Unny, T.E. (1973), "On the dynamic stability of fluid-conveying pipes", *J. Appl. Mech. -T ASME*, **40**(1), 48-52.
- Zhang, L.W., Song, Z.G., Qiao, P. and Liew, K.M. (2017), "Modeling of dynamic responses of CNT-reinforced composite cylindrical shells under impact loads", *Comput. Method. Appl. M.*, **313**, 889-903.

CC

## Appendix A

In this section, the micromechanics model is developed to examine the elastic properties of the single walled carbon nanotubes (SWCNTs)-reinforced polymeric composite. Some cases such as, straight and aligned CNTs and also two types of agglomeration by considering the effect of volume percent may be analyzed by applying the micromechanical model (Mori and Tanaka 1973). The experimental results reveal that the most of CNTs dispersion irregularly and centralize in spherical shapes in the matrix (Shi and Feng 2004). These regions are called "inclusions" which have different elastic properties from the matrix material.  $V_r$  is the total volume of CNTs which given as below

$$V_r = V_r^{inclusion} + V_r^m \quad (A1)$$

in which  $V_r^{inclusion}$  and  $V_r^m$  are the volumes of CNTs distributed in the spherical inclusions and in the matrix (concrete), respectively. Two following parameters are used to indicate the effect of agglomeration in the micromechanical model.

$$\xi = \frac{V_{inclusion}}{V}, \quad (A2)$$

$$\xi = \frac{V_{inclusion}}{V}, \quad (A3)$$

$C_r$  is the average volume fraction of CNTs in composite which is defined as follows

$$C_r = \frac{V_r}{V}. \quad (A4)$$

The volume fraction of the CNTs in the inclusions and in the matrix (concrete) can be related to each other as follows

$$\frac{V_r^{inclusion}}{V_{inclusion}} = \frac{C_r \xi}{\xi}, \quad (A5)$$

$$\frac{V_r^m}{V - V_{inclusion}} = \frac{C_r (1 - \xi)}{1 - \xi}. \quad (A6)$$

Assuming that the nanotubes are transversely isotropic and are distributed in the inclusions randomly, the inclusions are considered to be isotropic. Thereby, by applying Eshelby-Mori-Tanaka approach, the effective bulk modulus  $K$  and the effective shear modulus  $G$  of the isotropic materials can be written as below

$$K = K_{out} \left[ 1 + \frac{\xi \left( \frac{K_{in}}{K_{out}} - 1 \right)}{1 + \alpha (1 - \xi) \left( \frac{K_{in}}{K_{out}} - 1 \right)} \right], \quad (A7)$$

$$G = G_{out} \left[ 1 + \frac{\xi \left( \frac{G_{in}}{G_{out}} - 1 \right)}{1 + \beta(1 - \xi) \left( \frac{G_{in}}{G_{out}} - 1 \right)} \right], \quad (A8)$$

where  $K_{in}$  and  $K_{out}$  are the effective bulk modulus of the inclusion and the matrix outside the inclusion, respectively. Also,  $G_{in}$  and  $G_{out}$  are the effective shear modulus of the inclusion and the matrix outside the inclusion, respectively and are considered as follows

$$K_{in} = K_m + \frac{(\delta_r - 3K_m \chi_r) C_r \zeta}{3(\xi - C_r \zeta + C_r \zeta \chi_r)}, \quad (A9)$$

$$K_{out} = K_m + \frac{C_r (\delta_r - 3K_m \chi_r)(1 - \zeta)}{3[1 - \xi - C_r(1 - \zeta) + C_r \chi_r(1 - \zeta)]}, \quad (A10)$$

$$G_{in} = G_m + \frac{(\eta_r - 3G_m \beta_r) C_r \zeta}{2(\xi - C_r \zeta + C_r \zeta \beta_r)}, \quad (A11)$$

$$G_{out} = G_m + \frac{C_r (\eta_r - 3G_m \beta_r)(1 - \zeta)}{2[1 - \xi - C_r(1 - \zeta) + C_r \beta_r(1 - \zeta)]}, \quad (A12)$$

in which  $\chi_r, \beta_r, \delta_r$  and  $\eta_r$  can be calculated as

$$\chi_r = \frac{3(K_m + G_m) + k_r - l_r}{3(k_r + G_m)}, \quad (A13)$$

$$\beta_r = \frac{1}{5} \left\{ \frac{4G_m + 2k_r + l_r}{3(k_r + G_m)} + \frac{4G_m}{(p_r + G_m)} + \frac{2[G_m(3K_m + G_m) + G_m(3K_m + 7G_m)]}{G_m(3K_m + G_m) + m_r(3K_m + 7G_m)} \right\}, \quad (A14)$$

$$\delta_r = \frac{1}{3} \left[ n_r + 2l_r + \frac{(2k_r - l_r)(3K_m + 2G_m - l_r)}{k_r + G_m} \right], \quad (A15)$$

$$\eta_r = \frac{1}{5} \left[ \frac{2}{3}(n_r - l_r) + \frac{4G_m p_r}{(p_r + G_m)} + \frac{8G_m m_r(3K_m + 4G_m)}{3K_m(m_r + G_m) + G_m(7m_r + G_m)} + \frac{2(k_r - l_r)(2G_m + l_r)}{3(k_r + G_m)} \right]. \quad (A16)$$

Also,  $K_m$  and  $G_m$  are the bulk and shear modulus of the matrix phase which are given as below

$$K_m = \frac{E_m}{3(1 - 2\nu_m)}, \quad (A17)$$

$$G_m = \frac{E_m}{2(1 + \nu_m)}. \quad (A18)$$

Furthermore,  $\alpha$  and  $\beta$  which mentioned in Eqs. (A7) and (A8) are defined as follows

$$\alpha = \frac{(1 + \nu_{out})}{3(1 - \nu_{out})}, \quad (A19)$$

$$\alpha = \frac{(1 + \nu_{out})}{3(1 - \nu_{out})}, \quad (A20)$$

$$\nu_{out} = \frac{3K_{out} - 2G_{out}}{6K_{out} + 2G_{out}}. \quad (A21)$$

Eventually, the effective Young's modulus  $E$  and Poisson's ratio  $\nu$  of the composite are given by

$$E = \frac{9KG}{3K + G}, \quad (A22)$$

$$\nu = \frac{3K - 2G}{6K + 2G}. \quad (A23)$$

## Appendix B

By integrating the stress-strain relations of the structure (Eqs. (21)-(23)) we have

$$N_{xx} = A_{11} \left( \frac{\partial u}{\partial x} + \frac{1}{2} \left( \frac{\partial w}{\partial x} \right)^2 \right) + B_{11} \left( \frac{\partial \psi_x}{\partial x} \right) \quad (\text{B1})$$

$$+ A_{12} \left( \frac{\partial v}{R \partial \theta} + \frac{w}{R} + \frac{1}{2} \left( \frac{\partial w}{R \partial \theta} \right)^2 \right) + B_{12} \left( \frac{\partial \psi_\theta}{R \partial \theta} \right) + E_{31} \varphi,$$

$$N_{\theta\theta} = A_{12} \left( \frac{\partial u}{\partial x} + \frac{1}{2} \left( \frac{\partial w}{\partial x} \right)^2 \right) + B_{12} \left( \frac{\partial \psi_x}{\partial x} \right) \quad (\text{B2})$$

$$+ A_{22} \left( \frac{\partial v}{R \partial \theta} + \frac{w}{R} + \frac{1}{2} \left( \frac{\partial w}{R \partial \theta} \right)^2 \right) + B_{22} \left( \frac{\partial \psi_\theta}{R \partial \theta} \right) + E_{32} \varphi,$$

$$N_{x\theta} = A_{66} \left( \frac{\partial u}{R \partial \theta} + \frac{\partial v}{\partial x} + \frac{\partial w}{\partial x} \frac{\partial w}{R \partial \theta} \right) + B_{66} \left( \frac{\partial \psi_x}{R \partial \theta} + \frac{\partial \psi_\theta}{\partial x} \right), \quad (\text{B3})$$

$$Q_x = A_{55} \left( \frac{\partial w}{\partial x} + \psi_x \right) - E_{15} \frac{\partial \varphi}{\partial x}, \quad (\text{B4})$$

$$Q_\theta = A_{44} \left( \frac{\partial w}{R \partial \theta} - \frac{v}{R} + \psi_\theta \right) - E_{24} \frac{\partial \varphi}{R \partial \theta}, \quad (\text{B5})$$

$$M_{xx} = B_{11} \left( \frac{\partial u}{\partial x} + \frac{1}{2} \left( \frac{\partial w}{\partial x} \right)^2 \right) + D_{11} \left( \frac{\partial \psi_x}{\partial x} \right) \quad (\text{B6})$$

$$+ B_{12} \left( \frac{\partial v}{R \partial \theta} + \frac{w}{R} + \frac{1}{2} \left( \frac{\partial w}{R \partial \theta} \right)^2 \right) + D_{12} \left( \frac{\partial \psi_\theta}{R \partial \theta} \right) + F_{31} \varphi,$$

$$M_{\theta\theta} = B_{12} \left( \frac{\partial u}{\partial x} + \frac{1}{2} \left( \frac{\partial w}{\partial x} \right)^2 \right) + D_{12} \left( \frac{\partial \psi_x}{\partial x} \right) \quad (\text{B7})$$

$$+ B_{22} \left( \frac{\partial v}{R \partial \theta} + \frac{w}{R} + \frac{1}{2} \left( \frac{\partial w}{R \partial \theta} \right)^2 \right) + D_{22} \left( \frac{\partial \psi_\theta}{R \partial \theta} \right) + F_{32} \varphi,$$

$$M_{x\theta} = B_{66} \left( \frac{\partial u}{R \partial \theta} + \frac{\partial v}{\partial x} + \frac{\partial w}{\partial x} \frac{\partial w}{R \partial \theta} \right) + D_{66} \left( \frac{\partial \psi_x}{R \partial \theta} + \frac{\partial \psi_\theta}{\partial x} \right), \quad (\text{B8})$$

where the constants  $A_{ij}$ ,  $B_{ij}$ ,  $D_{ij}$ ,  $E_{ij}$  and  $F_{ij}$  are equal to

$$(A_{11}, A_{12}, A_{22}, A_{44}, A_{55}, A_{66}) = \int_{-h}^h (C_{11}, C_{12}, C_{22}, C_{44}, C_{55}, C_{66}) dz \quad (\text{B9})$$

$$+ \int_h^{h+h_p} (Q_{11}, Q_{12}, Q_{22}, Q_{44}, Q_{55}, Q_{66}) dz,$$

$$(B_{11}, B_{12}, B_{22}, B_{66}) = \int_{-h}^h (C_{11}, C_{12}, C_{22}, C_{66}) z dz \quad (\text{B10})$$

$$+ \int_{-h}^{h+h_p} (Q_{11}, Q_{12}, Q_{22}, Q_{66}) z dz,$$

$$(D_{11}, D_{12}, D_{22}, D_{66}) = \int_{-h}^h (C_{11}, C_{12}, C_{22}, C_{66}) z^2 dz \quad (\text{B11})$$

$$+ \int_{-h}^{h+h_p} (Q_{11}, Q_{12}, Q_{22}, Q_{66}) z^2 dz,$$

$$(E_{31}, E_{32}) = \frac{\pi}{h_p} \int_h^{h+h_p} (e_{31}, e_{32}) \cos \left( \frac{\pi(z-h)}{h_p} \right) dz, \quad (\text{B12})$$

$$(E_{15}, E_{24}) = \int_h^{h+h_p} (e_{15}, e_{24}) \sin \left( \frac{\pi(z-h)}{h_p} \right) dz, \quad (\text{B13})$$

$$(F_{31}, F_{32}) = \frac{\pi}{h_p} \int_h^{h+h_p} (e_{31}, e_{32}) \cos \left( \frac{\pi(z-h)}{h_p} \right) z dz, \quad (\text{B14})$$